

NASA Technical Memorandum 104550

11/47  
51122  
P-40

# Optically Thin Cirrus Clouds Over Oceans and Possible Impact on Sea Surface Temperature of Warm Pool in Western Pacific

C. Prabhakara, J.-M. Yoo, G. Dalu,  
and D. P. Kratz

November 1991

(NASA-TM-104550) OPTICALLY THIN CIRRUS  
CLOUDS OVER OCEANS AND POSSIBLE IMPACT ON  
SEA SURFACE TEMPERATURE OF WARM POOL IN  
WESTERN PACIFIC (NASA) 40 p CSCL 04B

N92-11600

Unclas  
0051122

G3/47

The NASA logo, consisting of the word "NASA" in a bold, sans-serif font.



**Optically Thin Cirrus Clouds Over  
Oceans and Possible Impact on  
Sea Surface Temperature of  
Warm Pool in Western Pacific**

**C. Prabhakara**  
*Goddard Space Flight Center  
Greenbelt, Maryland*

**J.-M. Yoo**  
*Applied Research Corporation  
Landover, Maryland*

**G. Dalu**  
*C.N.R.  
Istituto di Fisica dell' Atmosfera  
Rome, Italy*

**P. Kratz**  
*Universities Space Research Assn.  
Columbia, Maryland*



National Aeronautics and  
Space Administration

**Goddard Space Flight Center**  
Greenbelt, MD

1991

~~SECRET~~ INTENTIONAL ~~SECRET~~

## Table of Contents

1. Introduction .....	1
2. Satellite Observations of Thin Cirrus .....	3
3. Energy Balance Model for the Warmpool .....	20
4. Discussion and Conclusions .....	30
References .....	33

~~CONFIDENTIAL~~

## Abstract

Over the convectively active tropical ocean regions, the measurements made from space in the infrared and visible have revealed the presence of optically thin cirrus clouds, which are quite transparent in the visible and nearly opaque in the infrared. The Nimbus-4 Infrared Interferometer Spectrometer (IRIS), which has a field of view (FOV) of  $\approx 100$  km, has been utilized to examine the infrared optical characteristics of these cirrus clouds. From the IRIS data, it has been observed that these optically thin cirrus clouds prevail extensively over the "warm pool" region of the equatorial western Pacific, surrounding Indonesia. It is found that the seasonal cloud cover caused by these thin cirrus exceeds 50% near the central regions of the "warm pool." For most of these clouds, the optical thickness in the infrared is  $\leq 2$ . It is deduced that the dense cold anvil clouds associated with deep convection spread extensively and are responsible for the formation of the thin cirrus. This is supported by the observation that the coverage of the dense anvil clouds is an order of magnitude less than that of the thin cirrus. From these observations, together with a simple radiative-convective model, it is inferred that the optically thin cirrus can provide a greenhouse effect, which can be a significant factor in maintaining the "warm pool." In the absence of fluid transports, it is found that these cirrus clouds could lead to a runaway greenhouse effect. The presence of fluid transport processes, however, act to moderate this effect. Thus, if a modest  $20 \text{ W/m}^2$  energy input is considered to be available to warm the ocean, then it is found that the ocean mixed-layer of a 50-meter depth will be heated by  $\approx 1^\circ\text{C}$  in 100 days.



## 1. Introduction

The “warm pool” area, located in the equatorial western Pacific, has sea surface temperatures that exceed about  $28^{\circ}\text{C}$  in all seasons. As revealed by satellite measurements, the “warm pool” region is usually cloud-covered (Garcia, 1985) and is characterized by low values of the outgoing longwave radiation (OLR),  $\approx 200 \text{ W/m}^2$ . Moreover, in the “warm pool” region, the net radiation (the solar incoming minus OLR) at the top of the atmosphere is  $\approx 80 \text{ W/m}^2$  (Barkstrom et al., 1989). Another remarkable aspect of this region is that there is on the average about 10 mm/day of rain (Dorman and Bourke, 1979). By combining this salient information, together with a knowledge of the transports prevailing in the atmosphere and the ocean, up to a depth of the thermocline, it is possible to explain how the elevated temperatures in the “warm pool” are maintained. The errors in the estimation of the various energy processes at present, however, are such that it is difficult to draw definitive conclusions. To resolve this situation, the TOGA COARE (World Climate Research Program, 1989) program will make extensive measurements to help improve our understanding of the energy budget.

The purpose of the present study is to introduce a new mechanism, namely the radiative effects of thin cirrus clouds, to explain the energy balance of the “warm pool” region. The available evidence indicates that the impact of the thin cirrus clouds is to radiatively produce a local heat source, which appears to be a significant factor in maintaining the “warm pool”.

Several studies (e.g., Platt, 1989; Ramanathan et al., 1989; Stephens, 1980) have discussed the role of clouds in the atmosphere as regulators of the radiative energy balance. From observations, it has been deduced that clouds found primarily at low altitudes, such as stratiform clouds in the boundary layer, lead to a net cooling, since they reflect a significant percentage of the incoming solar energy while radiating to space in the infrared at fairly warm temperatures (Stephens and Webster, 1981). The

high altitude cirrus and cirrostratus clouds, however, radiate to space in the IR at a much cooler temperature which can result in a net warming. In the context of the global warming caused by increase in CO<sub>2</sub> and other trace gases, the role of the clouds in the atmosphere must be understood and properly taken into consideration.

Satellite observations in the infrared and visible (e.g., Hanel et al., 1972; Prabhakara et al., 1988; Inoue, 1985; Stowe et al., 1989) have revealed some of the interesting properties of the cold high altitude cirrus clouds that prevail over the “warm pool.” Other studies (Stephens, 1980; Platt et al., 1987) have also discussed the nature of the optically thin cirrus clouds. Platt et al. (1987) suggest that in the cold upper tropospheric regions, where there are small amounts of water vapor, the optically thin cirrus clouds present tend to be fairly transparent to incoming solar radiation while being nearly opaque to the outgoing infrared. These optical properties of the thin cirrus clouds have the potential to lead to a greenhouse warming. To date, the extent to which such a greenhouse warming is affecting the earth has not been assessed because of the lack of data concerned with the geographic extent of the thin cirrus and their infrared optical depth. Based on a recent study (Prabhakara et al., 1988), it is now possible to derive the necessary information from the data obtained by the Infrared Interferometer Spectrometer (IRIS) that was flown on Nimbus 4 satellite in 1970.

A brief account of the IRIS and a method to estimate the thin cirrus information is presented in Section 2. A simple radiative convective model that is applicable to the mesoscale convective systems in the “warm pool” is developed in Section 3. This radiative convective model, which does not explicitly take into account the transports, allows us to estimate the net heating in the presence of thin cirrus clouds.

## 2. Satellite observations of thin cirrus

The IRIS on board Nimbus 4 provided valuable data for about 10 months: April 1970 to January 1971. This spectrometer viewed the earth at nadir with a field of view of about 100 km and had a spectral resolution of  $2.8 \text{ cm}^{-1}$  in the IR region, 7 to  $25 \mu\text{m}$  (see Hanel et al., 1972, for more details on IRIS). In a study based on these high resolution IRIS data, Prabhakara et al. (1988) (hereafter called PFDWCS) inferred the presence of optically thin cirrus clouds over the convective areas of the oceans namely the “warm pool” region, the Intertropical Convergence Zone (ITCZ) and the South Pacific Convergence Zone (SPCZ).

From the IRIS observations, it is deduced that the thin cirrus clouds have a spatial scale of about a few hundred kilometers. Based on these observations, one can also infer that these thin cirrus clouds result from the spreading of the thick anvil clouds that have cold tops of  $\approx 220 \text{ K}$ . The scale of these complex cloud structures suggests that they are associated with mesoscale convective systems (MCS) that prevail in the convective areas.

In Figure 1, a schematic picture of the MCS over the “warm pool” area is shown with a mature cumulonimbus anvil and some cumulus clouds at low altitude in different stages of development. Under the outer reaches of the anvil there can be open ocean with no cumulus underneath. The IRIS spectra are well suited to distinguish the character of the cirrus clouds in the MCS. To demonstrate this point, a clear sky spectrum over the oceans and a spectrum of an oceanic scene containing an optically thin cirrus (PFDWCS) over the ocean are displayed in Figure 2 (a and b), respectively.

Unlike molecular absorption, which exhibits fine spectral structure, clouds tend to produce broad spectral features. A very prominent cloud extinction feature, namely an enhanced difference between the brightness temperatures at 11 and  $13 \mu\text{m}$ , can be readily identified and is located in the window region of the spectrum (see Figure 2b)

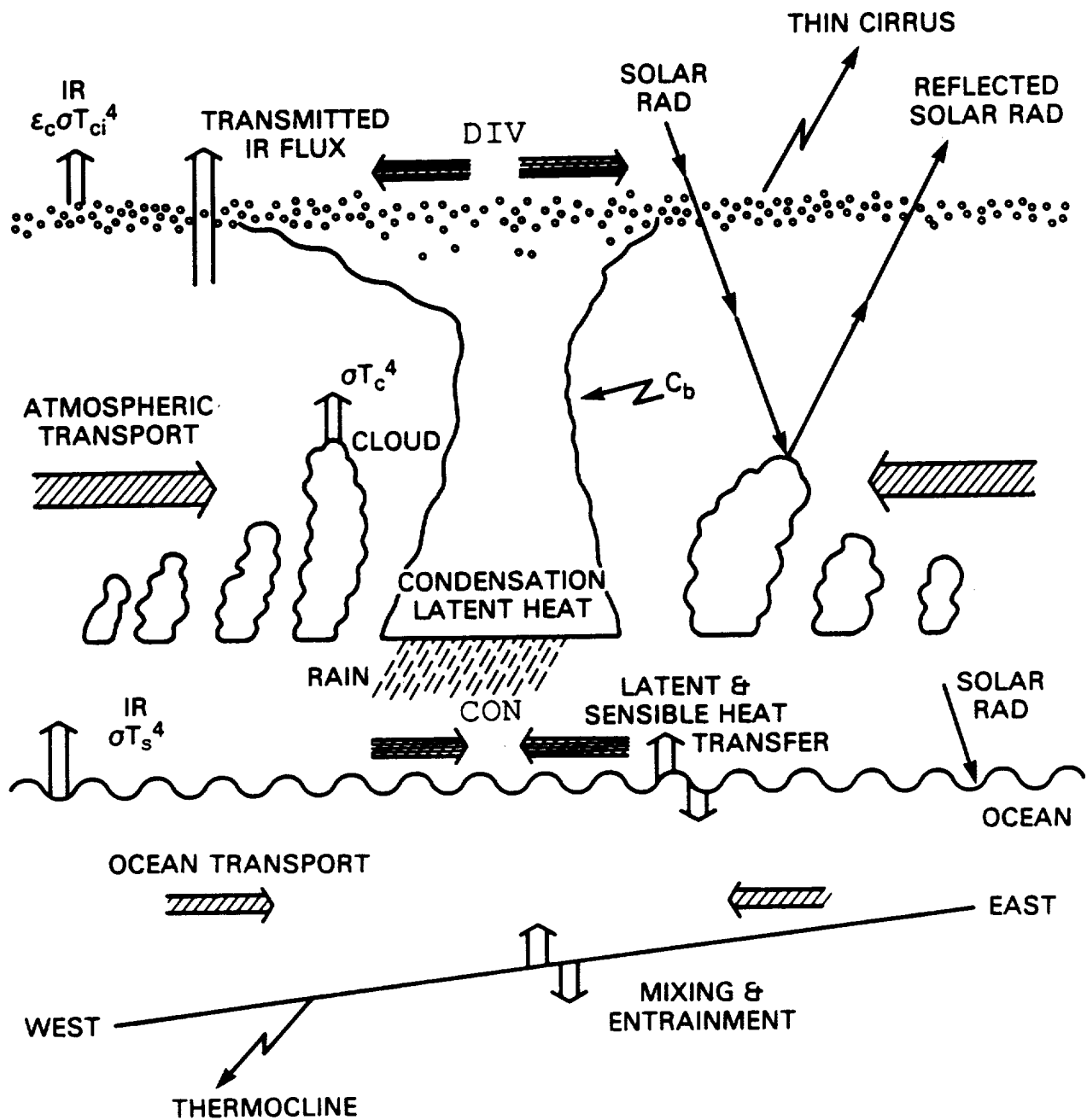


Figure 1. Schematic figure of the mesoscale convective system containing optically thin cirrus produced by spreading of deep convective cumulonimbus anvil. Depicted in the figure are a) weak cumulus underlying the cirrus, b) radiative processes at the sea surface and within the atmosphere, including cumulus and thin cirrus, and c) energy transports in the atmosphere and the ocean.

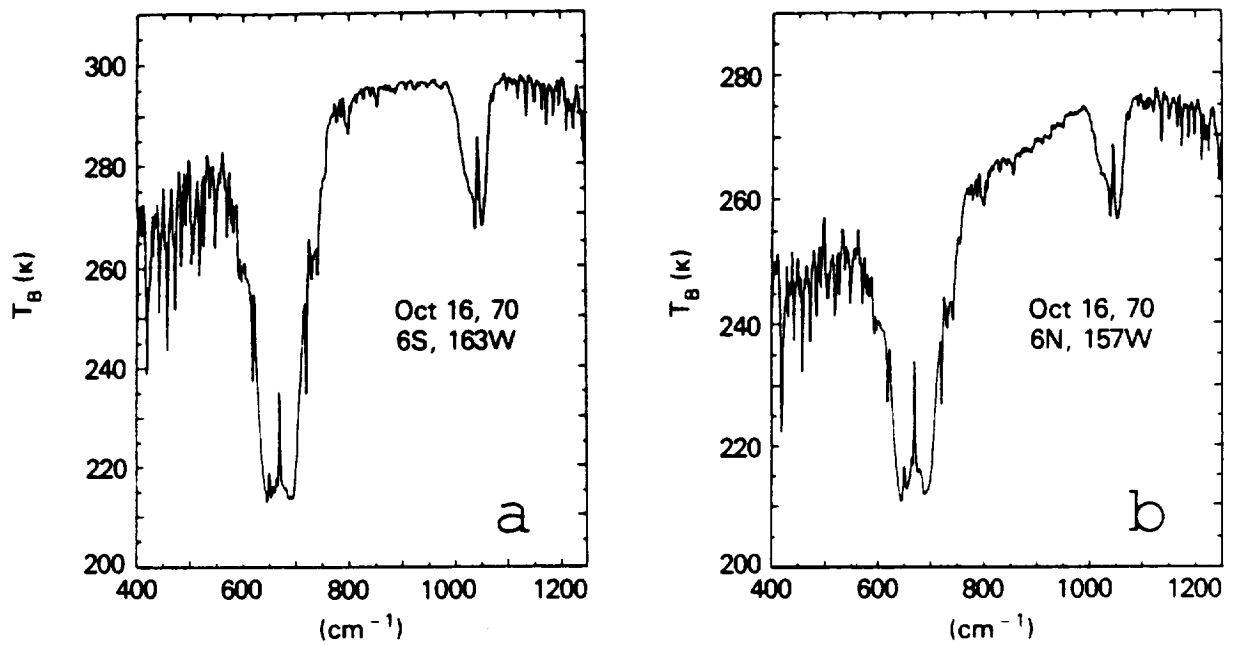


Figure 2. IRIS spectra observed over the tropical oceans.  
(a) Cloud-free tropical ocean spectrum.  
(b) Maritime tropical spectrum contaminated by optically thin cirrus.

between the 9.6  $\mu\text{m}$   $\text{O}_3$  band and the 15  $\mu\text{m}$   $\text{CO}_2$  band. The range of this cloud extinction feature stretches from 980 to 750  $\text{cm}^{-1}$  (10.2 to 12.9  $\mu\text{m}$ ). In addition, cloud extinction inferred from the IRIS spectra for the wavelength region from 18 to 25  $\mu\text{m}$ , where the water vapor rotation band is present, reinforces the conclusions drawn from the observations made in the window region.

Because of the presence of water vapor in the Earth's atmosphere, especially in the first few kilometers above the sea surface, the brightness temperature in the window region, for clear sky conditions, decreases from 980 to 775  $\text{cm}^{-1}$ . This decrease in brightness temperature from 11 to 13  $\mu\text{m}$ ,  $\Delta T = T_{11} - T_{13}$ , can be as large as 5°C in the humid "warm pool" region. Under these conditions, the value of  $T_{11}$  is about 293 K; however when there is an optically thin cirrus in the scene,  $\Delta T$  is significantly greater than 5°C and  $T_{11}$  is several degrees below 293 K. The brightness temperature in the rotation band region at 18  $\mu\text{m}$ ,  $T_{18}$ , is also reduced by thin cirrus. As shown in PFDWCS, the  $\Delta T$  in the optically thin cloud cases can be related to the cloud properties with the help of the radiative transfer theoretical calculations that take into account the absorption and scattering by the cirrus ice particles. Unlike the optically thin cloud, whose absorption is wavelength dependent, the optically thick cloud emits like a blackbody, and hence  $\Delta T$  is small. If we assume this optically thick cloud top is around 11 km, the brightness temperature at 11  $\mu\text{m}$  is some 70 K below the SST.

The discussion of the cloud spectra presented above is applied to a large MCS complex observed over the "warm pool" around local noon on October 16, 1970. In order to understand this case, twelve spectra observed by IRIS along one orbital track as the satellite passed northward from about 4°S, 167°E to 7°N, 164°E, are presented in Figure 3. Each of these spectra show some degree of cirrus cloud contamination, with the exception of the #7 near 0.3°N, which has the largest values of  $T_{11}$  and  $T_{18}$  (292 K and 267 K, respectively), and the smallest value of  $\Delta T$  (5.6 K). It is

OCT 16. 70

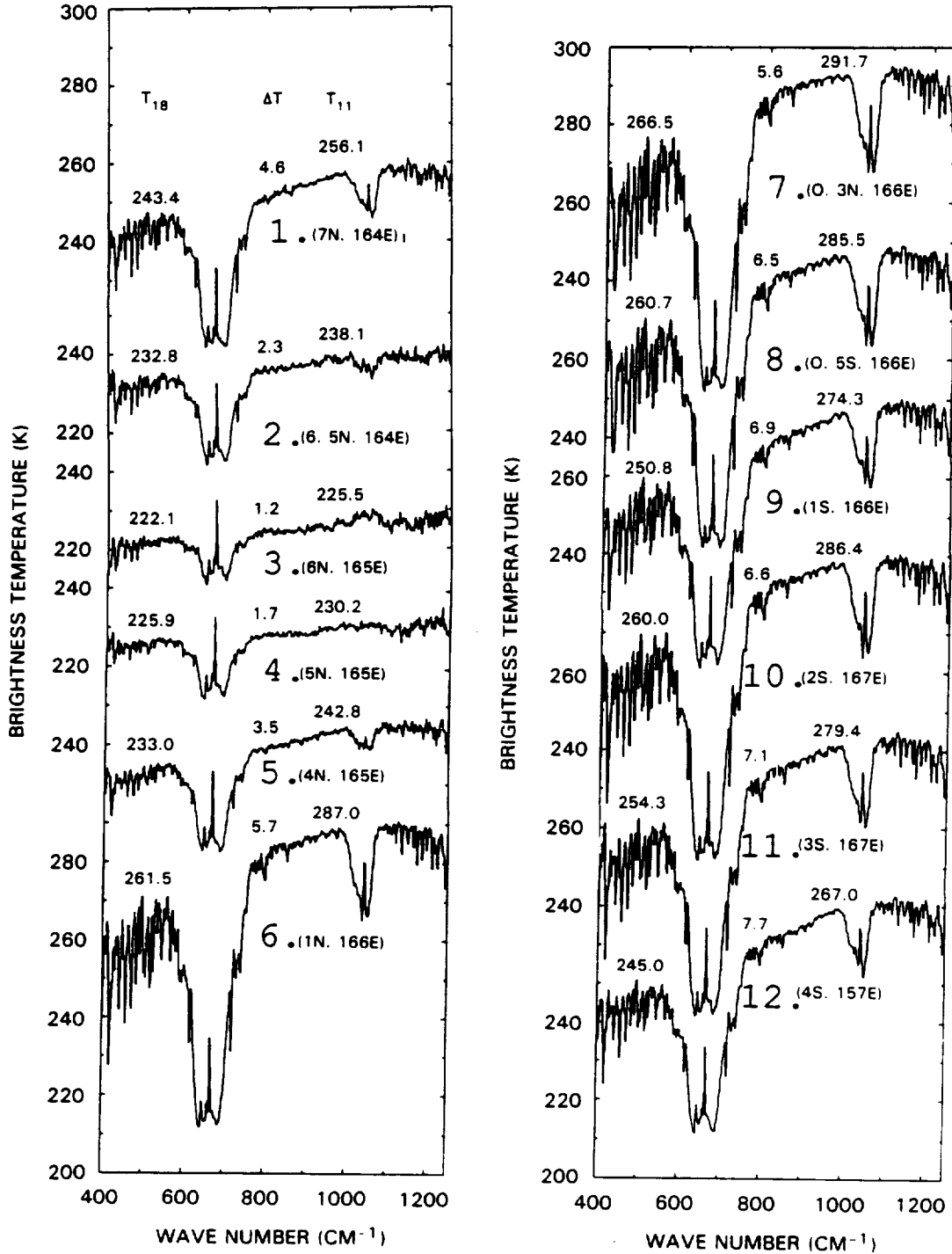


Figure 3. IRIS spectra observed along one orbital track as the satellite passed northward from about 4°S, 167°E to 7°N, 164°E on October 16, 1970. The spectra are numbered 1 to 12, starting with 7°N as 1 and ending with 4°S as 12. Each spectrum is identified with its location and spectral details pertaining to  $T_{10.8}$ ,  $\Delta T$  and  $T_{18}$ . The spectra are compacted along the ordinate with separate ordinate values.

straightforward to see that the spectra #3 and #4, where the 15  $\mu\text{m}$   $\text{CO}_2$  and the 9.6  $\mu\text{m}$   $\text{O}_3$  bands are weak and  $T_{11} \approx 225$  K, correspond to high cold clouds in the center of the MCS complex. The spectra on either side of the MCS center, i.e., #1 and #2, and #5 and #6 show a gradual warming and suggest a decrease in the effect of the dense clouds and an increase in the effect of the optically thin clouds. This is evident from the values of  $T_{11}$ ,  $\Delta T$ , and  $T_{13}$  identified in these spectra.

Spectra #8, #9, #10, #11, and #12 are influenced by some MCS that are outside the subsatellite track of the IRIS observations. The presence of the thin cirrus background in these spectra can be deduced, however, from their spectral characteristics (i.e.,  $T_{11}$ ,  $\Delta T$ , and  $T_{13}$ ). This can be appreciated by contrasting these spectra with that of spectrum #7. All of these cloud spectra give an indication of the massive aerial extent of thin cirrus over the "warm pool."

In the theoretical calculations, PFDWCS assumed the cirrus ice particles are spherical, having a log normal size distribution with an effective radius  $r_e$ . The value of brightness temperature calculated from this theoretical model for the relatively narrow spectral intervals at 11 and 13  $\mu\text{m}$  is shown to have the following functional dependence:

$$\begin{aligned} T_{11} &= f \{ (T_s - T_c), m, k_{11}(r_e), \omega_{11}(r_e) \} \\ T_{13} &= f \{ (T_s - T_c), m, k_{13}(r_e), \omega_{13}(r_e) \} \end{aligned} \quad (1)$$

where  $T_s$  is the sea surface temperature,  $T_c$  is the temperature of the cirrus cloud layer, which is assumed to be isothermal;  $m$  ( $\text{g}/\text{cm}^2$ ) is the mass of the ice particles in a column of the cloud;  $k_{11}$  and  $k_{13}$  ( $\text{cm}^2/\text{g}$ ) are the extinction cross sections of the ice particles in the cloud whose effective radius is  $r_e$ ; and  $\omega_{11}$  and  $\omega_{13}$  are the corresponding single scattering albedo values. It follows from Equation 1 that for a given  $(T_s - T_c)$  and  $r_e$ ,  $T_{11}$  and  $T_{13}$  are dependent on  $m$ , the mass of the particles in the cloud. Hence the difference  $\Delta T = T_{11} - T_{13}$  is also a function of  $m$ . Results of theoretical calculations (see PFDWCS) are illustrated in Figure 4 for a family of cirrus clouds with particle sizes  $r_e$  ranging between 1.5  $\mu\text{m}$  to 24  $\mu\text{m}$  and the total

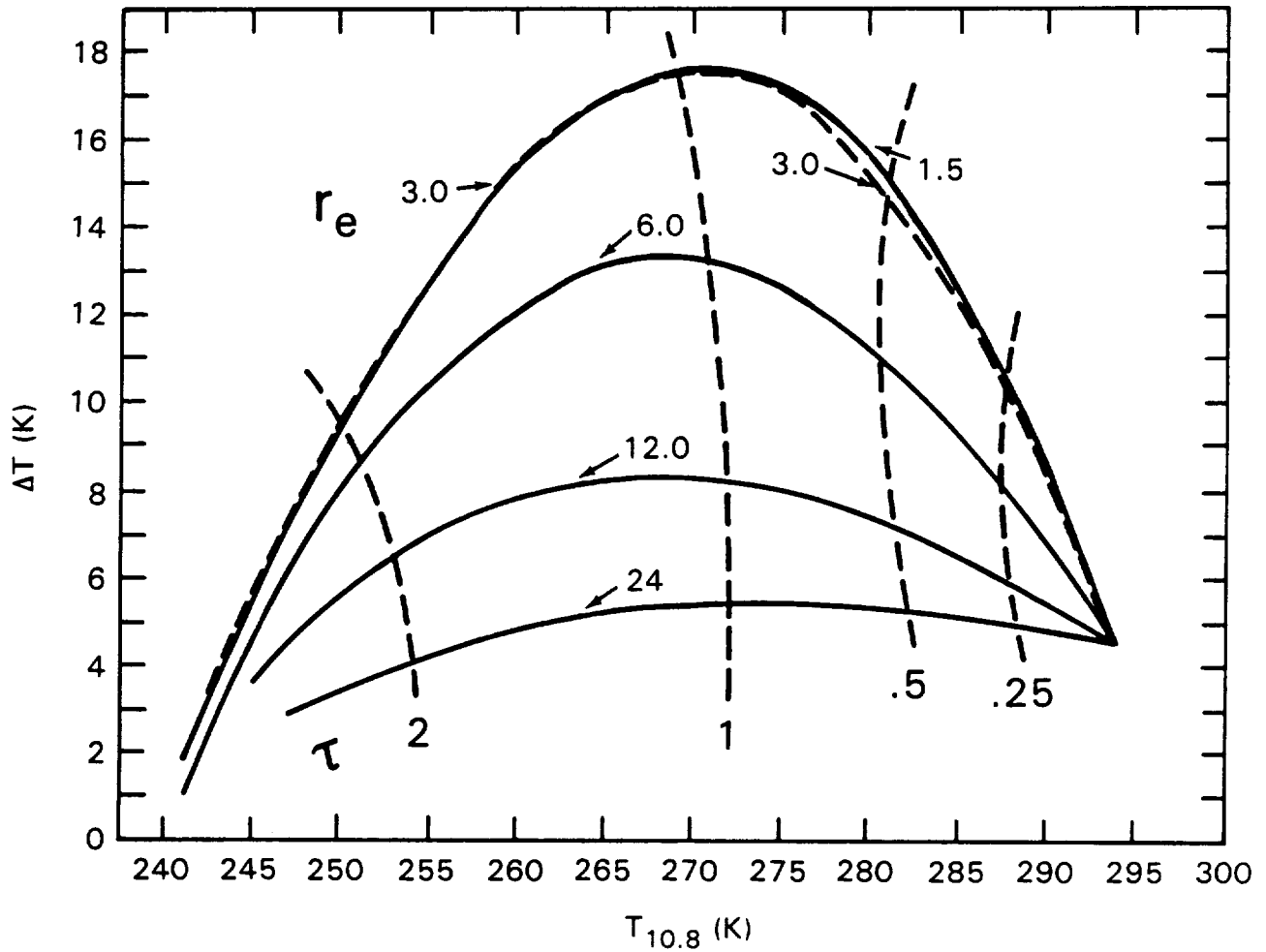


Figure 4. Theoretical values of  $\Delta T$  vs  $T_{10.8}$  for high-level (cirrus) spherical ice crystal clouds as a function of particle size and optical depth. The solid isolines of particle size  $r_e$  and dashed isolines of optical depth,  $\tau$  are identified. (Note: isoline of  $r_e = 3 \mu\text{m}$  is also dashed.)

extinction optical depth,  $\tau_{11}$ , ranging from 0 to 20. Underneath the cirrus, it is assumed there are no other clouds, and the surface temperature,  $T_s$ , is 301 K, while the temperature of the cirrus clouds,  $T_c$ , is taken to be 230 K. In Figure 4,  $\Delta T$  is plotted as a function of the brightness temperature  $T_{11}$  since both these quantities are measurable. It can be observed that the curves of  $\Delta T$  versus  $T_{11}$  for different values of  $r_e$  have a maximum  $\Delta T$  in the vicinity of  $T_{11} \approx 270$  K. This maximum is quite pronounced for small ice particles whose  $r_e \leq 6 \mu\text{m}$ . The isolines of optical depth  $\tau_{11}$  are shown in the Figure 4. These isolines reveal that  $\Delta T$  maximum is close to  $\tau_{11} = 1$ . An important result obtained from these theoretical calculations is that the extinction caused by the thin cirrus clouds is mainly responsible for decreasing  $T_{11}$  below 290 K and increasing  $\Delta T$  above 5 K. Water vapor absorption alone cannot explain such results.

In Figure 5 the IRIS observations over the tropical ocean ( $10^\circ\text{S}$  to  $10^\circ\text{N}$ ) are plotted as a function of  $\Delta T$  versus  $T_{11}$  to illustrate the correspondence between theory and observations.

In Figure 6 the theoretical frame work developed above is applied to the IRIS data over the equatorial Pacific. Here the IRIS observations, made during 3 months at four oceanic regions of  $10^\circ$  latitude  $\times 10^\circ$  longitude size, are presented in the form of frequency distribution in the space defined by the two variables  $\Delta T$  and  $T_{11}$ . Two of these oceanic regions represent the “warm pool” during the northern summer and fall seasons. The other two regions are chosen to reveal the character of the dry tropical eastern Pacific, where the subsidence in the atmosphere and the oceanic upwelling are dominant. The IRIS data over the “warm pool,” Figure 6 (a and b), when compared with the theoretical results, Figure 4, show some gross similarities. It should be noted that in observations involving diverse natural situations, other clouds such as cumulus (see Figure 1) may be present between the sea surface and cirrus, which can introduce a significant spread in the data presented in Figure 6 (a and b). Thus, one has to take

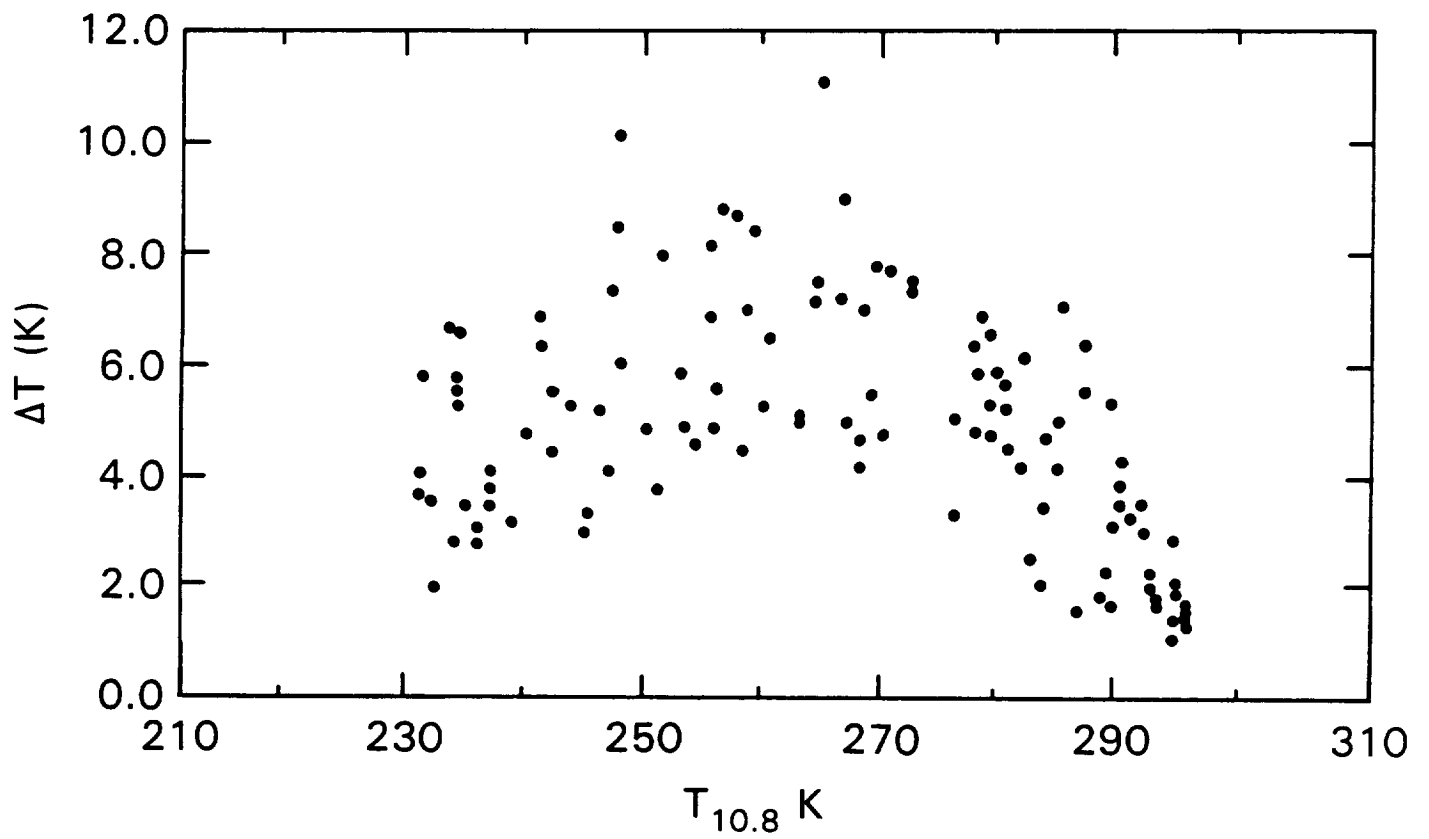
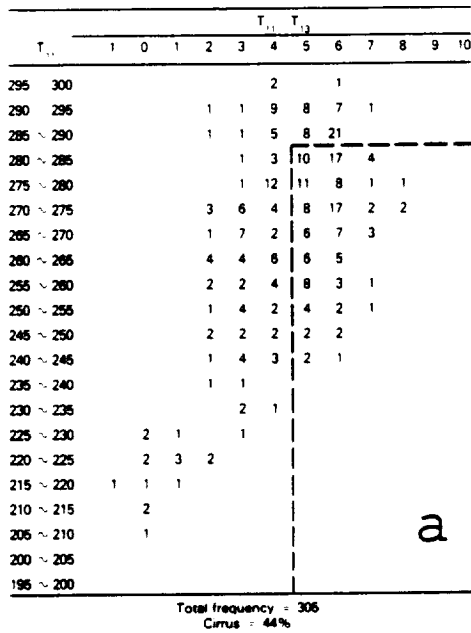


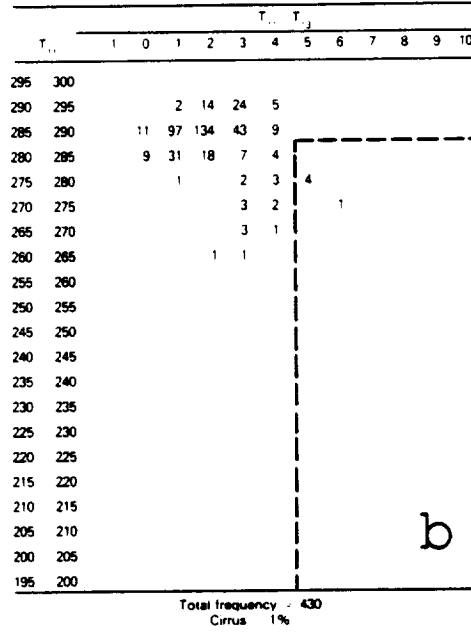
Figure 5. The temperature difference,  $\Delta T$ , vs  $T_{10.8}$  derived from the IRIS data over the tropical oceans ( $10^\circ\text{N}$  to  $10^\circ\text{S}$ ).

## SUMMER

Latitude: 5°N ~ 5°S, Longitude: 130°E ~ 140°E

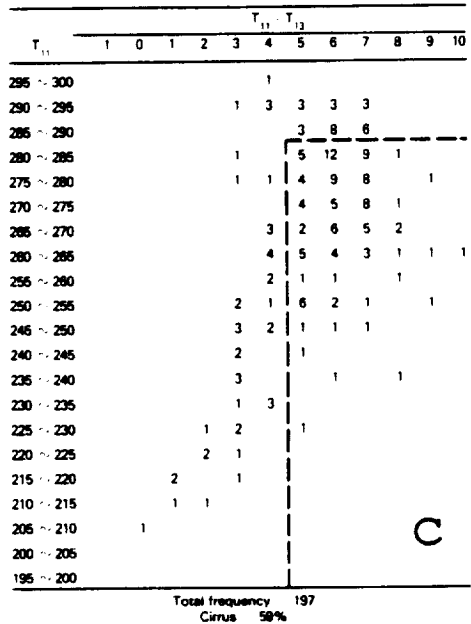


Latitude: 5°N ~ 5°S, Longitude: 90°W ~ 100°W



## FALL

Latitude: 5°N ~ 5°S, Longitude: 100°E ~ 110°E



Latitude: 5°N ~ 5°S, Longitude: 120°W ~ 130°W

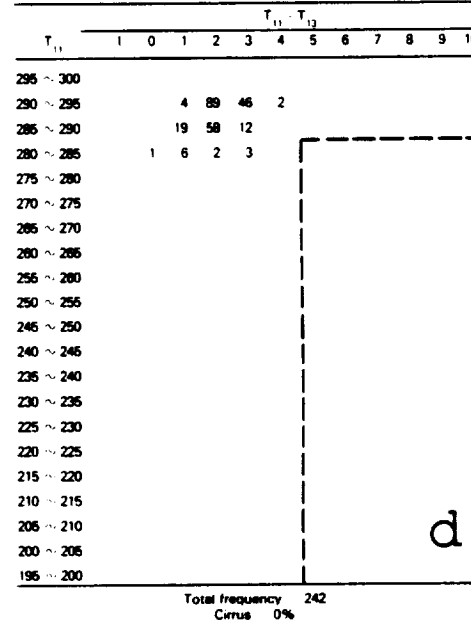


Figure 6. Frequency distributions of seasonal IRIS data as a function of  $\Delta T$  and  $T_{10.8}$  over the  $10^\circ$  latitude  $\times$   $10^\circ$  longitude oceanic regions for different seasons. Dashed vertical and horizontal lines delineate the thresholds on  $\Delta T$  and  $T_{10.8}$ . Both total frequency and cirrus percentage are also shown.

- (a) June, July, and August (5°N–5°S, 130°E–140°E).
- (b) June, July, and August (5°N–5°S, 90°W–100°W).
- (c) September, October and November (5°N–5°S, 100°E–110°E).
- (d) September, October and November (5°N–5°S, 120°W–130°W).

into consideration these variable conditions when comparing the theoretical results with the IRIS data. Despite these limitations, one observes that the  $\Delta T$  maximum in both the figures is close to  $T_{11} \approx 270$  K. The magnitude of  $\Delta T$  maximum of about 10 K in the data, when compared with that in Figure 4, suggests that  $r_e$  for such clouds is about  $6 \mu\text{m}$ .

The percentage cloud cover caused by thin cirrus and their optical depth can be estimated with the help of the analysis presented above. Based on the arguments presented earlier, if we assume the IRIS data shown in Figure 6 (a and b) (where  $T_{11} < 290$  K and  $\Delta T > 5$  K) represent thin cirrus in the whole field of view, then we can get an estimate of their percentage. Such estimates over the “warm pool” region are shown to reach  $\approx 60\%$ . On the contrary, over the dry subsidence regions, Figure 6 (c and d), the cirrus amount is negligibly small. Another important observation is that in the “warm pool” events, the high cold clouds  $T_{11} < 225$  K constitute only a small fraction  $\approx 5\%$  of the total number of cases.

Using this technique, the percentage of optically thin cirrus over the tropical oceans from  $25^\circ\text{N}$  to  $25^\circ\text{S}$  is deduced from IRIS measurements for four seasons as shown in Figure 7 (a–d). In order to illustrate the significance of the inferred thin cirrus, the climatology of sea surface temperature (SST) is shown in Figure 8 (a and b) for two seasons. The striking similarity between the distribution of thin cirrus clouds and the SST over the tropical oceans, and in particular over the “warm pool” region, is clearly revealed. Note that the maxima of these two variables move poleward during the local summer season.

A weighted mean optical depth of these thin cirrus clouds can be assessed as follows. If one takes the population of clouds with  $T_{11} < 290$  K and  $\Delta T > 5$  K, it is found that the weighted mean  $\bar{\tau}_{11}$  of such population is approximately 1.0 ( $\bar{\tau}_{11} = \sum \tau_i f_i / \sum f_i$ , where  $f_i$  is the frequency of observations, also note from Figures 4 and 6 that this population of cirrus clouds has  $2 > \tau_{11} > 0$ ).

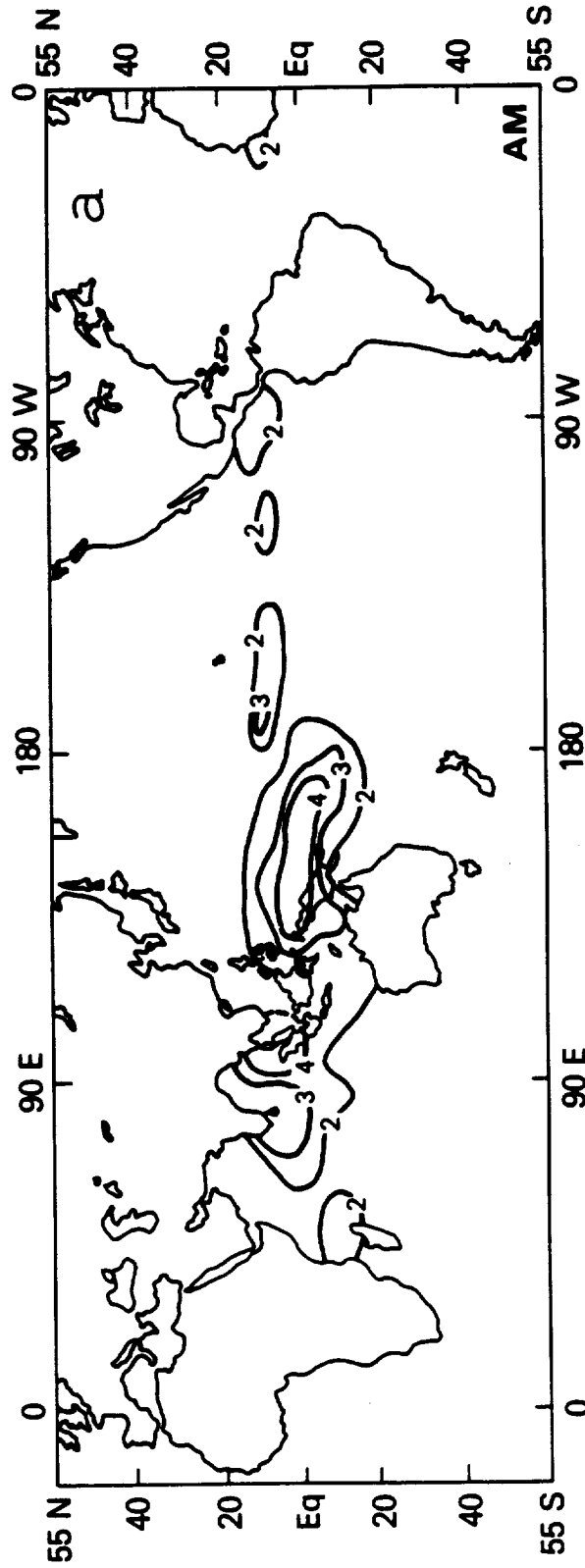


Figure 7(a). Seasonal percentage cloud cover caused by optically thin cirrus in the tropics between 25°N and 25°S during April and May. The numbers should be multiplied by 10 to get % cloud cover.

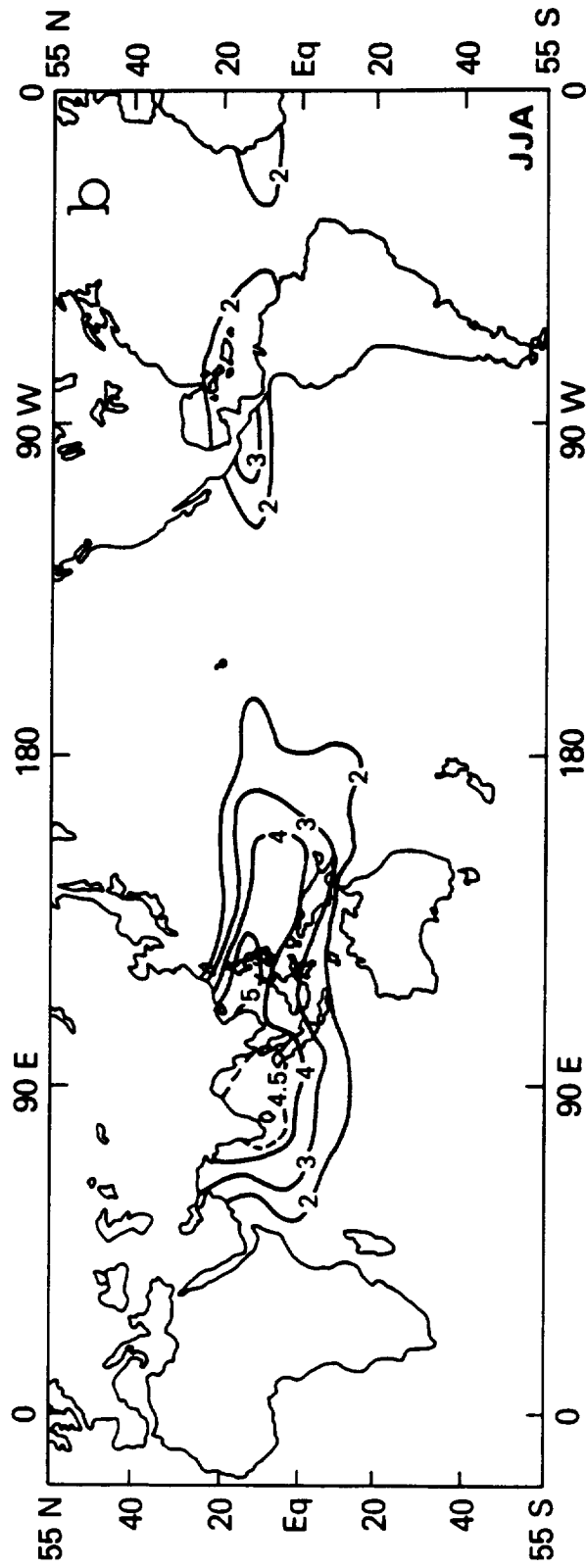


Figure 7(b). Seasonal percentage cloud cover caused by optically thin cirrus in the tropics between 25°N and 25°S during June, July, and August. The numbers should be multiplied by 10 to get % cloud cover.

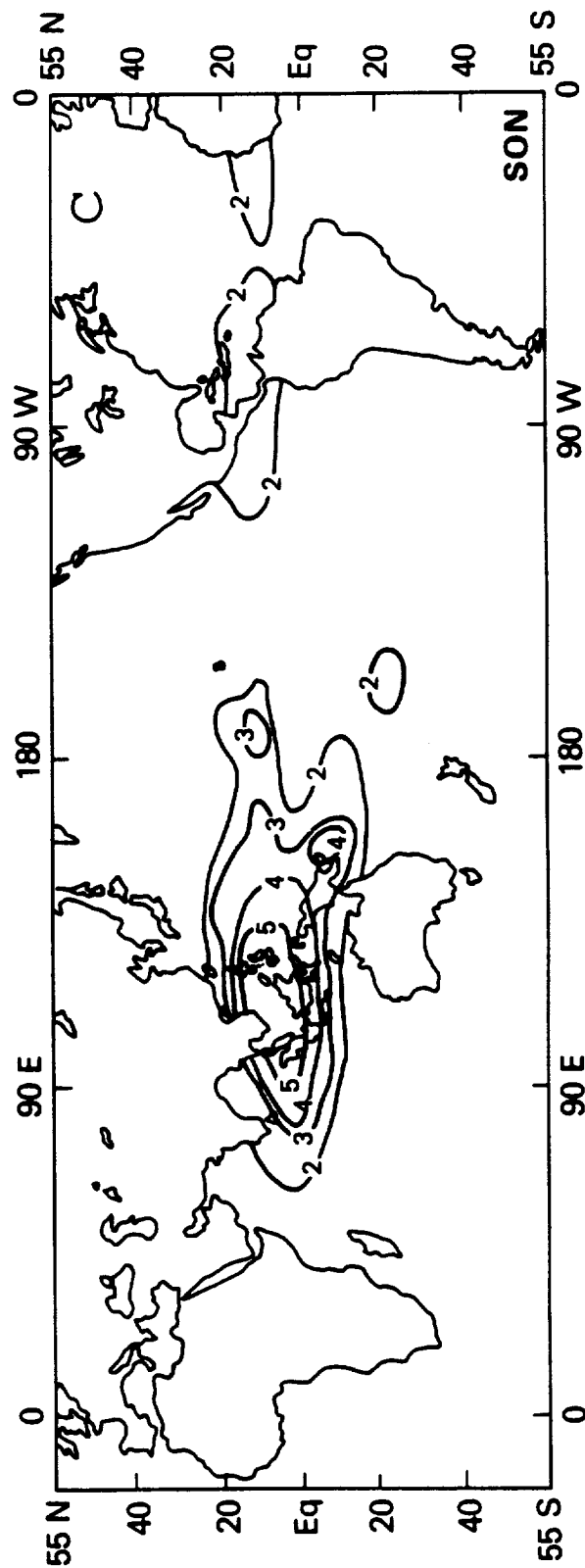


Figure 7(c). Seasonal percentage cloud cover caused by optically thin cirrus in the tropics between 25°N and 25°S during September, October, and November. The numbers should be multiplied by 10 to get % cloud cover.

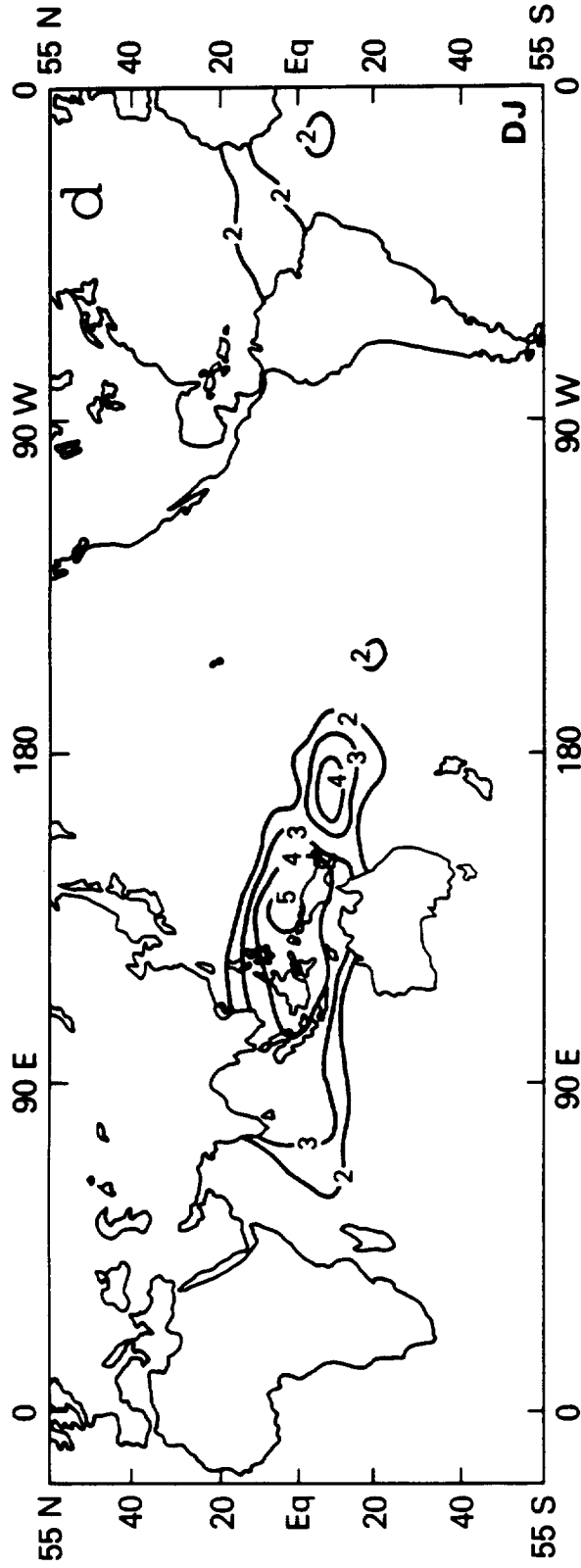


Figure 7(d). Seasonal percentage cloud cover caused by optically thin cirrus in the tropics between 25°N and 25°S during December and January. The numbers should be multiplied by 10 to get % cloud cover.

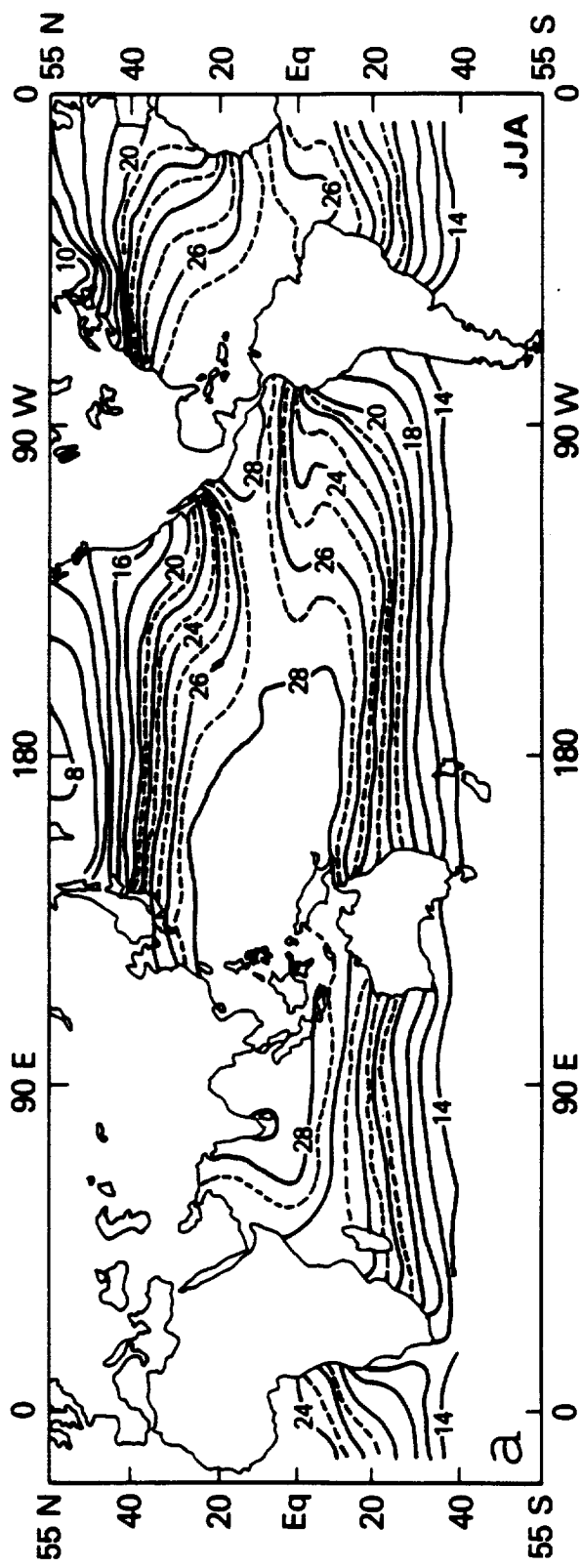


Figure 8(a). Climatological sea surface temperature °C (from World Climate Research Program, 1989) for June, July, and August.

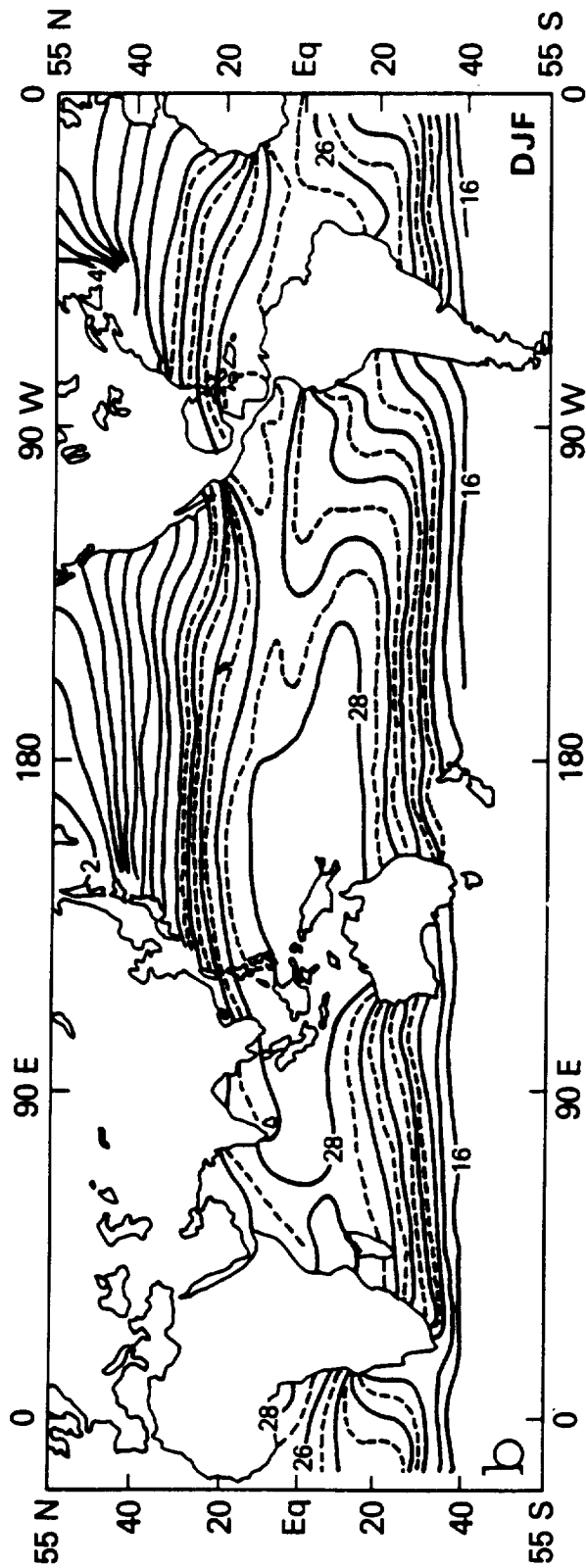


Figure 8(b). Climatological sea surface temperature °C (from World Climate Research Program, 1989) for November, December, and January.

### 3. Energy balance model for the “warm pool”

Optically thin cirrus clouds, which are more transparent in the visible than in the IR, are produced by MCS. They are present over an extensive area of the “warm pool” and therefore should have important implications to the local energy balance. The thermal structure, the convective cloudiness and precipitation in the atmosphere, as well as the temperature in the ocean up to a depth of the thermocline, could be impacted by this local energy balance. A comprehensive model that can explicitly take into account all the dynamical, physical and radiative processes pertaining to the coupled ocean-atmosphere system of the “warm pool” is beyond the scope of this study. Instead, a simple energy balance model is developed, which assumes implicitly the existence of convective transport, latent heating, and clouds that result from small-scale and large-scale dynamical processes in the “warm pool.” Given these salient conditions, a radiative energy balance model, which will be discussed, is considered to estimate the surface temperature.

It is assumed that the large-scale transport processes and convective motions in the tropics result in the formation of MCS's (see Figure 1). In the MCS's, some of the cumulonimbus clouds form anvils whose optically thin cirrus covers the sky completely. The lower tropospheric convective cumulus are taken to have cloud tops that reach an average altitude of 5.5 km. If we take the surface temperature to be 301 K and the lapse rate to be 6.5 K/km, then the cumulus cloud tops will have a temperature of 265 K. The cumulus clouds are taken to be blackbodies radiating at the cloud temperature. This means that the cumulus clouds emit 0.6 times the surface flux,  $\sigma T_s^4$ , where  $\sigma$  is the Stefan-Boltzmann constant. The cirrus are located near 12 km and are taken to have a negligible thickness. As before, if we take the surface temperature to be 301 K and the lapse rate to be 6.5 K/km, then the thin cirrus have a temperature of 223 K. This implies that if these thin cirrus were to radiate with an emissivity,  $\epsilon$ , then their emission would be equal to  $0.3\epsilon\sigma T_s^4$ . The cumulus

cloud cover,  $C$ , underneath the cirrus is an important parameter of the model and is allowed to vary. In our formulation, the IR emissivity of the cirrus is related to its visible albedo,  $\alpha$ , with the help of radiometer measurements obtained from aircraft flights (Spinherne and Hart, 1990) as shown in Table 1. The IR transmissivity of the cirrus is given by  $(1 - \epsilon)$ , and its visible transmissivity is  $(1 - \alpha)$ . In these calculations, the visible reflectivity of the cumulus,  $r$ , is allowed to vary between 0.55 and 0.65 (e.g., Stowe et al., 1988), the visible albedo is varied from 0.0 to 0.4, and the cumulus fraction, from 0.0 to 0.9. A scheme for the radiative processes in the model is presented in Figure 9. As shown by Equation 2, the energy balance between the incoming solar radiation and the outgoing longwave radiation at the top of the atmosphere can be described by:

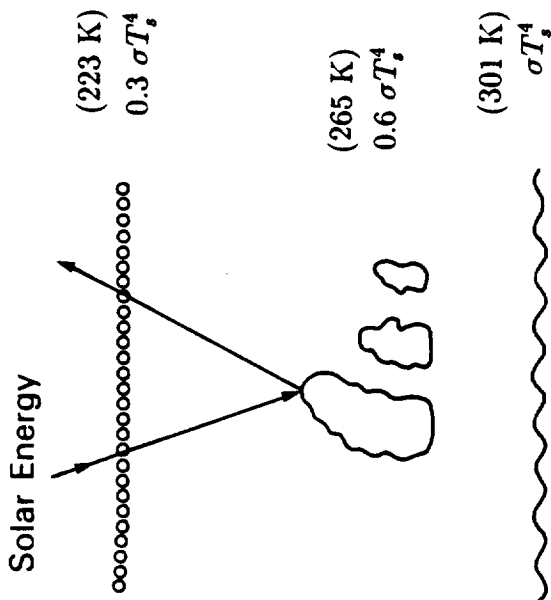
$$\begin{aligned}
 G_1 \sigma T_s^4 (\epsilon t' + A) + (1 - \epsilon) [0.6 C G_2 \sigma T_s^4 + (1 - C) G_3 \sigma T_s^4] \\
 = S(1 - \alpha) \{ [1 - \alpha_s (1 - \alpha)] (1 - C) + [1 - r(1 - \alpha)] C \},
 \end{aligned}
 \tag{2}$$

where  $S$  is the solar constant, and  $\alpha_s$  is the albedo of the cloud free atmosphere and the ocean surface. The first term on the left-hand side gives the IR emission from the cirrus and the overlying atmosphere containing  $\text{CO}_2$ ,  $\text{O}_3$ , and  $\text{H}_2\text{O}$ . The IR flux transmission of the atmospheric absorbing gases above the cirrus level is expressed as  $t' = 0.94$ . The constant,  $A = 0.06$ , arises because of the emission of the atmosphere above the cirrus. The constant,  $G_1$ , represents the ratio  $(T_c/T_s)^4$ , which is 0.30. The second term on the left-hand side represents the IR radiation emerging through the cirrus. This term has two components: a) a part that corresponds to the emission from the cumulus, and the atmospheric gases between cumulus top and cirrus, and b) a part that represents the emission from the surface and the atmosphere underlying the cirrus. In here the emission from the cumulus region is weighted by the cumulus fraction,  $C$ , and the rest, by  $(1 - C)$ . The constants  $G_2$  and  $G_3$  are scaling constants that are meant to scale the emission from a) and b), respectively. This scaling is done to express the emission from these layers in terms of the blackbody radiation from

Table 1. Relationship Between the Visible Albedo and Infrared Emissivity of Cirrus

$\alpha$	$\epsilon$
0.0	0.00
0.1	0.36
0.2	0.63
0.3	0.78
0.4	0.88
0.5	0.94

SIMPLE ENERGY BALANCE MODEL



Visible Reflectivity of Cumulus    0.55    0.65  
 or  
 Transmissivity of Cirrus for Visible    0.8    0.7

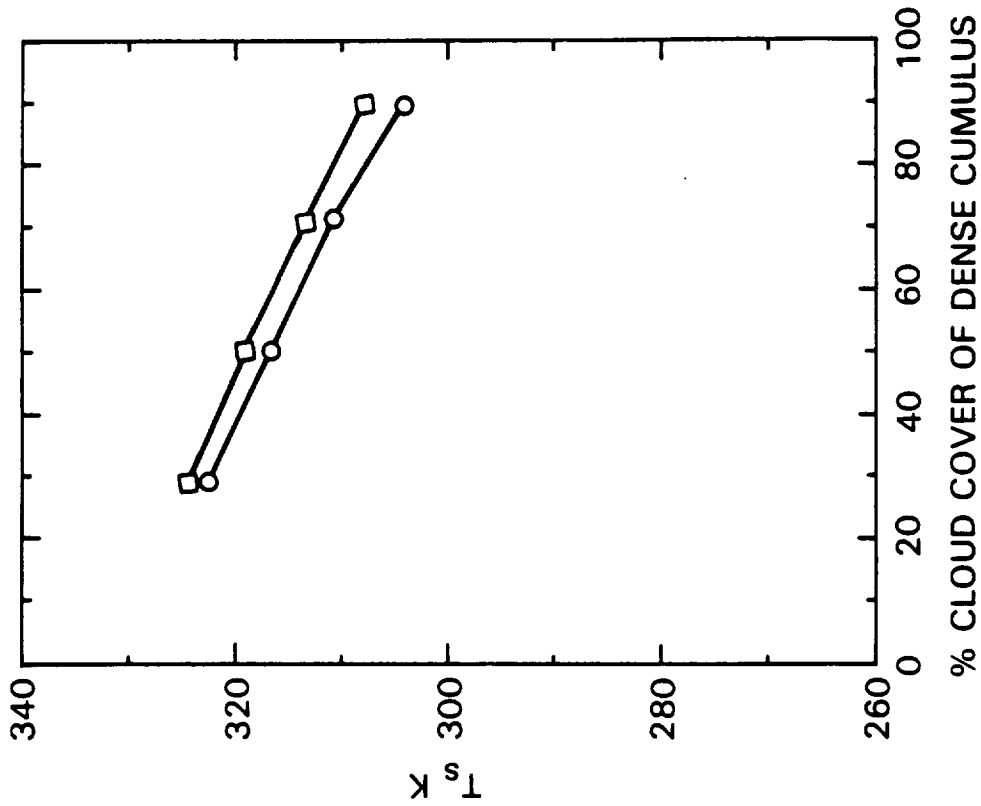


Figure 9. (Left panel) Schematic diagram showing the energy balance model and its vertical structure in this study. (Right panel) Surface temperature  $T_s$ , computed according to Equation 3. The curve with the symbol “o” is for cumulus reflection  $r = 0.55$  and cirrus visible transmission = 0.8 (i.e.  $\alpha = 0.2$ ). The curve with the symbol “o” stands for  $r = 0.65$  and cirrus visible transmission = 0.7 (i.e.  $\alpha = 0.3$ ).

the surface,  $\sigma T_s^4$ . The values of  $G_2$  and  $G_3$  are 0.83 and 0.63, respectively. These constants, as well as  $t'$  and  $A$ , are obtained from IR radiative transfer computations for a tropical atmosphere, assuming  $T_s = 301$  K, lapse rate of 6.5 K/km, 5 g/cm<sup>2</sup> of water vapor, a tropical ozone profile with 0.28 cm of O<sub>3</sub> and a tropopause temperature of 190 K at 17 km.

The term on the right-hand side of Equation 2 is an approximation for the incoming solar energy that is absorbed by the surface-atmosphere system. This absorption, for clear sky conditions within the tropics, leads to an effective radiative temperature at the top of the atmosphere near 270 K. This estimate of the effective radiative temperature in the tropics is consistent with that obtained in other studies (e.g., Stephens and Webster, 1981). From Equation 2, one can solve for the surface temperature,  $T_s$ , as a function of  $C$  and  $\alpha$ , given the magnitude of the other variables. For present purposes, the diurnal mean insolation near the equator is taken to be  $S = 405$  W/m<sup>2</sup>. Based on satellite measurements,  $\alpha_s$  is taken to be 0.10 (e.g., Gill, 1982). Equation 2 may be simplified as follows:

$$\beta \sigma T_s^4 = (1 - \alpha_c)S,$$

$$\text{where } \beta = [G_1(\epsilon t' + A) + (1 - \epsilon)\{0.6CG_2 + (1 - C)G_3\}] \quad (3)$$

$$\text{and } \alpha_c = [\alpha_s((1 - C)(1 + \alpha^2) + 2\alpha C) + (1 - 2\alpha_s)\alpha + rC(1 - \alpha)^2].$$

In Equation 3,  $\alpha_c$  is equivalent to an effective albedo and  $\beta$  is the effective emissivity of the earth atmosphere system. From Equation 3, one notes that the ratio  $(1 - \alpha_c)/\beta$  may be interpreted as a greenhouse amplification factor that takes into account not only the effect of the gases but also the strong interaction of clouds on IR and solar radiation.

Taking  $r = 0.55$  in Equation 2,  $T_s$  is estimated for different values of  $C$  and  $\alpha$ . These values of  $T_s$  are presented in Table 2(a). The corresponding values of  $\alpha_c$  and  $\beta$ , as defined by Equation 3, are listed in Tables 2(b and c, respectively).

Table 2. Results Obtained from Equation 3 as a Function of the Cirrus Albedo  $\alpha$  and the Cumulus Fraction  $C$

(a)

$\alpha \backslash C$	0.0	0.1	0.3	0.5	0.7	0.9
0.0	317.8	315.4	310.1	303.9	296.7	288.1
0.1	327.1	324.7	319.5	313.7	307.1	299.4
0.2	334.1	331.7	326.6	321.0	314.9	307.9
0.3	334.2	332.0	327.3	322.2	316.7	310.7
0.4	330.0	328.0	323.8	319.3	314.6	309.5

(b)

$\alpha \backslash C$	0.0	0.1	0.3	0.5	0.7	0.9
0.0	0.10	0.15	0.24	0.33	0.42	0.51
0.1	0.18	0.22	0.29	0.36	0.44	0.51
0.2	0.26	0.29	0.35	0.41	0.47	0.52
0.3	0.35	0.37	0.42	0.46	0.50	0.55
0.4	0.44	0.45	0.49	0.52	0.55	0.58

(c)

$\alpha \backslash C$	0.0	0.1	0.3	0.5	0.7	0.9
0.0	0.63	0.62	0.59	0.57	0.54	0.51
0.1	0.51	0.50	0.49	0.47	0.45	0.44
0.2	0.42	0.42	0.41	0.40	0.39	0.38
0.3	0.37	0.37	0.36	0.36	0.35	0.35
0.4	0.34	0.34	0.34	0.33	0.33	0.33

Note: in Equation 3 the cumulus and cirrus temperatures are coupled to the surface temperature. (a) Surface temperature  $T_s$ . (b) Effective albedo  $\alpha_e$ . (c) Effective emissivity  $\beta$ .

From Table 2(a), one notes that in the absence of cumulus and cirrus clouds, the radiative-convective equilibrium leads to a surface temperature of 316.1 K. This warm temperature of the equatorial ocean results from the greenhouse effects of the atmospheric gases such as CO<sub>2</sub> and H<sub>2</sub>O. It must be noted, however, that this assumes the absence of fluid transports. If the effects of clouds are taken into consideration, it is observed that since the cumulus cloud fraction is increased to 0.9 with no cirrus present, the surface temperature drops to 287.8 K. If optically thin cirrus clouds with  $\alpha = 0.2$  (i.e.,  $\epsilon = 0.63$ ) are now included in the scene, the surface temperature is raised to a value of 307.7 K [see Table 2(a)]. This example demonstrates the effect of the thin cirrus veil on the sea surface temperature.

When the incoming solar energy is not in balance with the OLR, there will be a net radiative energy input,  $E_{net}$ , at the top of the atmosphere. This input may be estimated by the following simple expression when  $\alpha_c$ ,  $\beta$ , and  $T_s$  are given:

$$E_{net} = S(1 - \alpha_c) - \beta\sigma T_s^4. \quad (4)$$

Taking the values of  $\alpha_c$  and  $\beta$  from Table 2(b and c), and the surface temperature,  $T_s = 301$  K, from observations of the “warm pool” region, we have estimated the net energy input,  $E_{net}$ . The values of  $E_{net}$  that are calculated from Equation 4 are presented in Table 3. One notes that the maximum net input of energy into the ocean atmosphere system occurs when the cirrus visible albedo is about 0.2. Based on the approximations developed by Platt and Stephens (1980), we can relate this emissivity to a total optical depth of approximately one for the cirrus cloud. These optimal conditions of energy input are apparently present in the “warm pool” region, as evidenced by the IRIS observations (see Figures 5 and 6), which show that the bulk of the cirrus clouds have optical depths around unity. One may also note from Table 1 that the cumulus clouds generally decrease the net energy input to the system.

Following the path of maximum net energy input, which corresponds closely to  $\alpha = 0.2$ , we find from Table 3 that when  $C \approx 0.2$ , the input energy is about 80 W/m<sup>2</sup>.

Table 3. Net Energy Input at the Top of the Atmosphere ( $E_{net}$ )  
 Calculated According to Equation 4 as a Function of Cirrus Albedo  
 and Cumulus Fraction  $C$  When the Surface Temperature  $T_s$   
 is a Constant ( $T_s = 301$  K)

$\alpha \backslash C$	0.0	0.1	0.3	0.5	0.7	0.9
0.0	71.0	58.8	34.5	10.1	-14.2	-38.5
0.1	93.5	82.6	60.9	39.1	17.3	-4.4
0.2	101.4	92.0	73.2	54.3	35.5	16.6
0.3	90.1	82.5	67.3	52.1	36.9	21.7
0.4	70.2	64.4	52.7	41.0	29.4	17.7

Table 4. Same as Table 2(a) except the Cumulus and Cirrus Temperatures  
 are not Coupled to the Surface and are Given a Constant Value  
 of 265 K and 223 K, Respectively

Reflectivity  $r$  of cumulus is 0.55.

$\alpha \backslash C$	0.0	0.1	0.3	0.5	0.7	0.9
0.0	317.8	316.6	313.1	306.4	288.7	*
0.1	333.0	332.5	331.1	328.5	322.2	283.1
0.2	354.9	355.3	356.2	358.0	361.9	379.8
0.3	374.3	375.3	377.9	382.5	392.7	434.4
0.4	395.7	396.9	400.2	406.1	419.0	470.1

\* The case where  $\alpha = 0$  and  $C = 0.9$  is physically unrealistic since the incoming solar energy is insufficient to balance the outgoing IR when the cumulus cloud temperature is 265 K.

This combination of cirrus and cumulus yields  $\alpha_c \approx 0.33$  [see Table 2(b)]. These estimates of the albedo,  $\alpha_c$ , and net energy input of  $\approx 80 \text{ W/m}^2$  are consistent with the Earth Radiation Budget Satellite (ERBS) observations reported by Barkstrom et al. (1989).

In Figure 9, two curves are shown, which illustrate the dependence of the sea surface temperature,  $T_s$ , on the cumulus cloud fraction,  $C$ , which is calculated according to Equation 2. These curves correspond to a)  $r = 0.55$ ,  $\alpha = 0.2$  and b)  $r = 0.65$ ,  $\alpha = 0.3$ . The first case is contained in Table 2. Although no table is presented for the second case, it is noted that when  $\alpha = 0.2$  and  $C = 0.2$ , an increase in  $r$  from 0.55 to 0.65 results in a drop of the net input energy from  $\approx 80 \text{ W/m}^2$  to  $\approx 75 \text{ W/m}^2$ . This example demonstrates the sensitivity of  $E_{net}$  to the value of  $r$  while Table 3 gives the sensitivity of  $E_{net}$  to  $C$  and  $\alpha$ .

To convey the significance of the energy input, we take as an example a case where only  $20 \text{ W/m}^2$  of the net radiative energy at the top of the atmosphere is available to heat the ocean water. We find that for these conditions, an ocean mixed layer of 50 meter depth will be heated by about  $1^\circ\text{C}$  in 100 days. Measurements from the TOGA COARE program of the surface energy balance over the "warm pool" region will be valuable in validating our conclusions.

The radiative convective model adopted here may be scrutinized further. In particular, one may examine the parameterization of the cumulus and cirrus cloud temperatures that are scaled in terms of the surface temperature. This parameterization forces the cumulus and cirrus cloud temperatures to increase approximately by factors of 0.6 and 0.3, respectively, of the surface temperature increase. Thus, for small perturbations of  $T_s$ , taking a constant lapse rate, one can note that the altitude and the pressure level of the clouds remain virtually unchanged. In this coupled cloud temperature system, as the surface temperature increases, infrared loses

to space increases from both the surface and the clouds. This has a moderating effect on  $T_s$  variations. If, however, as a counter example, we take the temperature of the cumulus and cirrus clouds to be constant, then the heights of the clouds will increase as  $T_s$  increases. Moreover, the infrared loss to space will depend mainly on  $T_s$ , and thus as a consequence, for a given increase in infrared opacity (such as that caused by an increase in the  $\text{CO}_2$  abundance) of the atmosphere and clouds,  $T_s$  will increase by a larger amount than that in the scaled cloud temperature case (see Table 4). This constant cloud temperature scenario leads to a runaway greenhouse effect more quickly than the scaled cloud temperature scenario. The two formulations considered here are anticipated to cover a reasonable range of conditions. Thus, from the results presented here, we expect that the coupled surface and cloud temperature model, which we adopted, will yield conservative estimates of the surface temperature variations.

#### 4. Discussion and conclusions

Satellite cloud pictures in the visible channel show almost perpetual cloudiness over the western Pacific equatorial regions around Indonesia. These clouds have the potential to block a significant amount of solar input energy. Furthermore, it is well known from climatology that the western equatorial Pacific is a region of heavy precipitation as well as being the area with the warmest sea surface temperature. The coexistence of these clouds and warm waters requires an explanation. The TOGA COARE program, in which several components of the energy balance pertaining to the “warm pool” region will be measured, is attempting to explain this. The aim of this study is to show that optically thin cirrus clouds, which emanate from the anvils of convective storms in the “warm pool” and cover the area extensively with sufficient optical depth in the IR, can account for a significant net solar energy input locally into this atmosphere-ocean system. This net input, amounting to about  $80 \text{ W/m}^2$ , may be largely responsible for the maintenance of the “warm pool” regime.

Another important factor is the rainwater addition. The low density rainwater in the top layers of the ocean (Lukas, 1988), together with weak wind stress, helps to maintain stable stratification and promote heating. Thus the ocean atmosphere system in the “warm pool,” through a set of positive feedback mechanisms, retains a significant amount of solar energy to keep itself operating. A schematic diagram of the various dynamic and physical processes that lead to the formation of the “warm pool” system is presented in Figure 10. The two physical processes—namely, the optically thin cirrus and the addition of fresh rain water in the top layer of the ocean, i.e., a freshwater lens—are coupled to the “warm pool” and aid in its maintenance. A clear implication of this schematic figure is that the solar energy, through monsoonal scale interactions and by localized heating aided by the thin cirrus, is directly responsible for the maintenance of the “warm pool.”

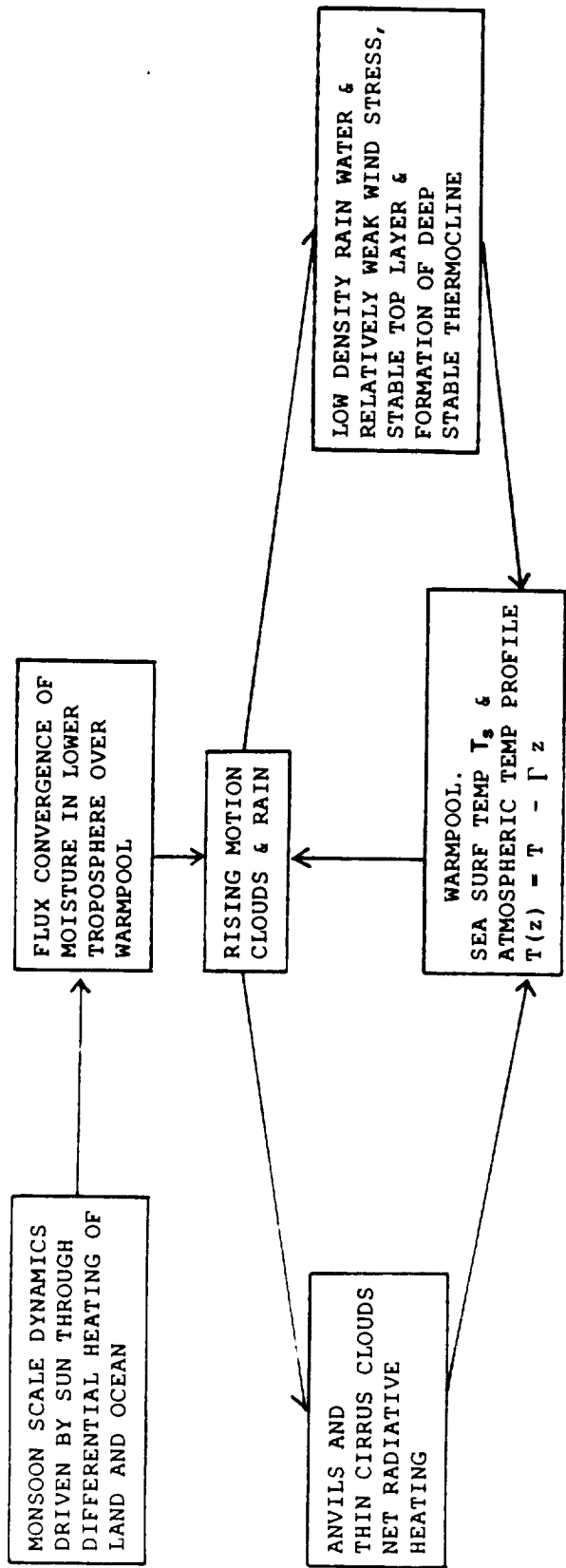


Figure 10. Flow diagram for physical processes in the convectively active oceanic regions responsible for maintaining the warm pools.

On a global scale, considerations of energy balance lead to the conclusion that, although the sun is the ultimate source of energy, the greenhouse effect produced by gases such as  $\text{H}_2\text{O}$ ,  $\text{CO}_2$  and  $\text{O}_3$  is important in maintaining the relatively warm surface temperatures for the Earth. While the transport processes in the atmosphere and oceans are primarily responsible for reducing the thermal contrast between the tropics and polar regions, they have a relatively minor influence on the global mean temperature. For these reasons, a radiative convective equilibrium model (e.g., Arking, 1991; Ramanathan and Coakley, 1978) which does not consider the large scale fluid transports may be used to calculate the global mean surface temperature assuming a tropospheric temperature profile that follows a prescribed lapse rate.

In a localized region, the fluid transport processes can have a significant influence on heat and moisture. If these processes are very rapid, then the effect of any local energy input caused by radiative convective processes will be reduced to a negligible level. On the other hand, if these transports are not rapid then a discernable temperature rise will result. Based on the satellite observations pertaining to a net radiative energy input of  $\approx 80 \text{ W/m}^2$  and to the thin cirrus clouds, that can enhance the greenhouse effect, we have inferred that the “warm pool” region has a source of net radiative input and has a directly driven circulation. This forms the basis for our simple radiative convective equilibrium model for the “warm pool” region. The current model is self-consistent and yields an understanding of the radiative and dynamic interactions prevailing in this region along with an explanation for surface temperature.

## References

Arking, A., 1991. The radiative effects of clouds and their impact on climate. *Bull. Amer. Meteor. Soc.*, In press.

Barkstrom, B., E. Harrison, G. Smith, R. Green, J. Kibler, R. Cess, and the ERBE Science Team, 1989. Earth radiation budget experiment (ERBE) Archival and April 1985 results. *Bull. Amer. Meteor. Soc.*, **70**, 1254-1262.

Dorman, C.E., and R.H. Bourke, 1979. Precipitation over the Pacific Ocean, 30°S to 60°N. *Mon. Wea. Rev.*, **107**, 896-910.

Garcia, O., 1985. Atlas of highly reflective clouds for the global tropics: 1971-1983. U.S. Dept. of Commerce, NOAA, Environmental Research Lab., Boulder, Co.

Gill, A.E., 1982. *Atmosphere-Ocean Dynamics*. Academic Press, 662 pp.

Hanel, R.A., B.J. Conrath, V.G. Kunde, C. Prabhakara, I. Revah, V.V. Salomonson, and G. Wolford, 1972. The Nimbus 4 infrared spectroscopy experiment 1. Calibrated thermal emission spectra. *J. Geophys. Res.*, **77**, 2629.

Inoue, T., 1985. On the temperature and effective emissivity determination of semi-transparent cirrus clouds by bi-spectral measurements in the 10 um window region. *J. Met. Soc. Japan*, **63**, 88-89.

Lukas, R., 1988. On the role of western Pacific air-sea interaction in the El Nino/Southern Oscillation Phenomenon. In Proceedings of the U.S. TOGA Western Pacific Air-Sea Interaction Workshop Honolulu, 16-18 September, 1987. R. Lukas and P. Webster, eds., *U.S. TOGA Rept. USTOGA-8, U. Corp. Atmos. Res.*, 43-69.

Platt, C.M.R., 1989. The role of cloud microphysics in high-cloud feedback effects on climate change. *Nature*, **341**, 428-429.

Platt, C.M.R., and G.L. Stephens, 1980. The interpretation of remotely sensed high cloud emittances. *J. Atmos. Sci.*, **37**, 2314-2322.

Platt, C.M.R., J.C. Scott, and A.C. Dille, 1987. Remote sensing of high clouds. Part VI: Optical properties of midlatitude and tropical cirrus. *J. Atmos. Sci.*, **44**, 729-747.

Prabhakara, C., R.S. Fraser, G. Dalu, Man-Li C. Wu, R.J. Curran distribution over oceans deduced from Nimbus 4 IRIS. *J. Appl. Meteor.*, **27**, 379-399.

Ramanathan, V., R.D. Cess, E.F. Harrison, P. Minnis, B.R. Barkstrom, E. Ahmad, and D. Hartmann, 1989. Cloud-radiative forcing and climate: Results from the earth radiation budget experiment. *Science*, **243**, 57-63.

Ramanathan, V., and J.A. Coakley, Jr, 1978. Climate modeling through radiative convective models. *Rev. Geophys. Space Phys.*, **16**, 465-489.

Spinhirne, J.D., and W.D. Hart, 1990. Cirrus structure and radiative parameters from airborne lidar and spectral radiometer observations: The 28 October 1986 FIRE study. *Mon. Wea. Rev.*, **118**, 2329-2343.

Stephens, G.L., 1980. Radiative properties of cirrus clouds in the infrared region. *J. Atmos. Sci.*, **37**, 435-446.

Stephens, G.L., and P.J. Webster, 1981. Clouds and climate: Sensitivity of simple systems. *J. Atmos. Sci.*, **38**, 235-247.

Stowe, L.L., C.G. Wellemeyer, T.F. Eck, H.Y.M. Yeh, and the Nimbus-7 Cloud Data Processing Team, 1988. Nimbus-7 global cloud climatology. Part I: Algorithm and validation. *J. Climate*, **1**, 445-470.

Stowe, L.L., H.Y.M. Yeh, T.F. Eck, C.G. Wellemeyer, H.L. Kyle and the Nimbus-7 Cloud Data Processing Team, 1989. Nimbus-7 global cloud climatology. Part II: First year results. *J. Climate*, **2**, 671-709.

World Climate Research Programme, 1989. A coupled ocean-atmosphere response experiment for the warm pool regions of the western Pacific. Scientific plan for the TOGA coupled ocean-atmosphere response experiment (COARE). Draft July 1989, 111 pp.

REPORT DOCUMENTATION PAGE			Form Approved OMB No. 0704-0188	
Public reporting burden for this collection of information is estimated to average 1 hour per response, including the time for reviewing instructions, searching existing data sources, gathering and maintaining the data needed, and completing and reviewing the collection of information. Send comments regarding this burden estimate or any other aspect of this collection of information, including suggestions for reducing this burden, to Washington Headquarters Services, Directorate for Information Operations and Reports, 1215 Jefferson Davis Highway, Suite 1204, Arlington, VA 22202-4302, and to the Office of Management and Budget, Paperwork Reduction Project (0704-0188), Washington, DC 20503.				
1. AGENCY USE ONLY (Leave blank)	2. REPORT DATE November 1991	3. REPORT TYPE AND DATES COVERED Technical Memorandum		
4. TITLE AND SUBTITLE Optically Thin Cirrus Clouds Over Oceans and Possible Impact on Sea Surface Temperature of Warm Pool in Western Pacific			5. FUNDING NUMBERS	
6. AUTHOR(S) C. Prabhakara, J.-M. Yoo, G. Dalu, and D. P. Kratz				
7. PERFORMING ORGANIZATION NAME(S) AND ADDRESS(ES) Goddard Space Flight Center Greenbelt, Maryland 20771			8. PERFORMING ORGANIZATION REPORT NUMBER  92B00006 Code 913	
9. SPONSORING/MONITORING AGENCY NAME(S) AND ADDRESS(ES) National Aeronautics and Space Administration Washington, D.C. 20546-0001			10. SPONSORING/MONITORING AGENCY REPORT NUMBER  NASA TM-104550	
11. SUPPLEMENTARY NOTES Prabhakara: Goddard Space Flight Center, Greenbelt, MD; Yoo: Applied Research Corporation, Landover, MD; Dalu: C.N.R., Istituto di Fisica dell' Atmosfera, Rome, Italy; and Kratz: Universities Space Research Association, Columbia, MD.				
12a. DISTRIBUTION / AVAILABILITY STATEMENT  Unclassified-Unlimited  Subject Category 47			12b. DISTRIBUTION CODE	
13. ABSTRACT (Maximum 200 words)  Over the convectively active tropical ocean regions, the measurements made from space in the infrared and visible have revealed the presence of optically thin cirrus clouds, which are quite transparent in the visible and nearly opaque in the infrared. The Nimbus-4 Infrared Interferometer Spectrometer (IRIS), which has a field of view (FOV) of $\approx 100$ km, has been utilized to examine the infrared optical characteristics of these cirrus clouds. From the IRIS data, it has been observed that these optically thin cirrus clouds prevail extensively over the "warm pool" region of the equatorial western Pacific, surrounding Indonesia. It is found that the seasonal cloud cover caused by these thin cirrus exceeds 50% near the central regions of the "warm pool." For most of these clouds, the optical thickness in the infrared is $\leq 2$ . It is deduced that the dense cold anvil clouds associated with deep convection spread extensively and are responsible for the formation of the thin cirrus. This is supported by the observation that the coverage of the dense anvil clouds is an order of magnitude less than that of the thin cirrus. From these observations, together with a simple radiative-convective model, it is inferred that the optically thin cirrus can provide a greenhouse effect, which can be a significant factor in maintaining the "warm pool." In the absence of fluid transports, it is found that these cirrus clouds could lead to a runaway greenhouse effect. The presence of fluid transport processes, however, act to moderate this effect. Thus, if a modest $20 \text{ W/m}^2$ energy input is considered to be available to warm the ocean, then it is found that the ocean mixed-layer of a 50-meter depth will be heated by $\approx 1^\circ\text{C}$ in 100 days.				
14. SUBJECT TERMS Warm pool; Cirrus clouds; Greenhouse effect			15. NUMBER OF PAGES 42	
			16. PRICE CODE	
17. SECURITY CLASSIFICATION OF REPORT Unclassified	18. SECURITY CLASSIFICATION OF THIS PAGE Unclassified	19. SECURITY CLASSIFICATION OF ABSTRACT Unclassified	20. LIMITATION OF ABSTRACT	